



Simulation of cold heavy oil production using an integrated modular approach with emphasis on foamy oil flow and sand production effects

J. WANG, D. A. WALTERS
Taurus Reservoir Solutions Ltd.

A. SETTARI, R. G. WAN
University of Calgary

This paper has been selected for presentation and publication in the Proceedings at the 1st Heavy Oil Conference. All papers selected will become the property of WHOC. The right to publish is retained by the WHOC's Publications Committee. The authors agree to assign the right to publish the above-titled paper to WHOC, who have conveyed non-exclusive right to the Petroleum Society to publish, if it is selected.

Abstract

In this paper, the authors extend earlier work on sand production modeling to incorporate the foamy oil effect, and present an integrated modular approach to quantitatively predict volumetric sand production and enhanced oil recovery. This model is based on mixture theory with erosion mechanics, in which multiphase hydrodynamics and geomechanics are coupled in a consistent manner via principal unknowns, such as saturation, pressure, porosity, and formation displacements. Foamy oil is modeled as a dispersion of gas bubbles trapped in the oil, where these gas bubbles maintain a higher reservoir pressure. A modular approach is then adopted to effectively take advantage of the existing advanced standard reservoir and stress-strain codes. The model is implemented into three integrated computational modules, i.e. erosion module, reservoir module, and geomechanics module. The stress, flow and erosion equations are solved separately for each time increment, and the coupling terms (porosity, permeability, plastic shear strain, etc) are passed among them and iterated until certain convergence is achieved on a time step basis. The system is powerful in terms of its capabilities, yet practical in terms of computer requirements and maintenance. Numerical

results of field studies are presented to illustrate the capabilities of the model. The effects of foamy oil flow and sand production are also examined to demonstrate their impact on the enhanced hydrocarbon recovery.

Introduction

Cold Heavy Oil Production with Sand (CHOPS) has become a successful non-thermal recovery process, and has been applied to enhance heavy oil production all over the world. This primary recovery method was pioneered in Alberta, Canada, and then gradually spread over China, Venezuela and Kazakhstan where heavy oils are mainly deposited. CHOPS uses operating techniques and specialized pumping equipment (progressing cavity pumps with surface drives) to aggressively produce heavy oil. Due to low operating costs and relatively high recovery factors by comparing to the thermal recovery method, CHOPS has become an economical mainstream strategy of heavy oil recovery. The primary enhanced recovery mechanisms are commonly believed to be sand production creating wormholes and foamy oil drive once the oil falls below the bubble point.

Removal of unconsolidated reservoir sand

During the cold heavy oil production, dynamic erosion process occurs at wellbore perforation tips. The sand particles are eroded away due to the combination of low material strength of the unconsolidated reservoir formation and aggressive high-pressure drawdown. The oil or gas flow transports the failed fine sand particles to the surface facilities, while leaving the coarse ones in the wellbore (removed by progressive cavity pumps). The removal of large quantities of sand particles (debris) creates a system of wormholes (elongated channels) or cavities that have been confirmed by numerous oil operators and researchers from field tracer test, and sand pack lab experiments⁽¹⁾⁽²⁾. Sanding results in, but not limited to, reduction of life cycles of equipments, stability of a wellbore, treatment of unwanted sand in an environmentally acceptable manner. On the other hand, limited sand production has been proven to significantly increase the well productivity when tolerating it at a manageable level. With limited sand production, well productivity could be 10-20 times higher than no-sand controlled conditions. Typical CHOPS wells produce 5-25 m³/day of oil with as much as 150-300 m³ of sand in the early years of production⁽³⁾.

Foamy oil behavior

The basic foamy oil characteristic is believed to be the existence of a “pseudo” bubble point⁽⁴⁾. The true bubble point pressure is reached when the first small bubbles of free gas evolve from solution in the oil and nucleate as a distinct free gas phase at the reservoir temperature. For conventional oils the gas rapidly coalesces into large bubbles and forms immediately a separate and distinct gas phase due to relatively low viscosity of conventional oils. The bubble point and the “pseudo” bubble point have the same or very close to the same values which is measured in a PVT cell in the laboratory. While in case of foamy oils, the gas bubbles cannot immediately coalesce together to form bubbles large enough to allow gravitational forces to separate them from the oil due to the high oil viscosity. The solution gas bubbles are entrained as foam in the oil. Therefore, the oil phase remains as a continuous dispersed gas-oil emulsion with a higher concentration of increasingly larger bubbles trapped in a milkshake-like format within the oil as the reservoir pressure decreases. The bubbles of free gas can finally start to escape from solution as a distinct free gas phase when the pressure further decreases. This pressure is known as the pseudo bubble point pressure. The delayed free gas production maintains a higher reservoir pressure. Hence, foamy oil reservoir pressure delivers greater primary recovery with less reservoir pressure decline and lower GOR's⁽⁵⁾.

Geomechanical effects

Geomechanics has been gaining much attention in explaining many phenomena such as reservoir compaction, subsidence, wellbore stability, pore collapse, and sand production. In CHOPS, after the reservoir formation around the wellbore has failed due to either shear or tensile failure caused by the imposed stress changes due to drawdown, the production of sand occurs as a by-product of hydrocarbon recovery. After mobilized sand is produced, sand arches are bound to form behind the perforation opening. The arches could be destroyed subject to flow drawdown changes. Each destabilization of the arches causes sanding peaks over the production period. The removal of sand particles also degrades the material strength of the reservoir formation. The stress field is further modified and the vertical stress must be re-distributed into the horizontal directions.

In summary, the effects mentioned above act interactively during the hydrocarbon production. Sand production is initially triggered by the continuous yielding of the formation around the wellbore under the combined effects of stress re-distribution, gas evolution and hydro-dynamical forces. The removal of sand particles modifies the wellbore geometry and the effective permeability of the formation is increased. This results in an enhanced well productivity. When the bottom hole pressure is lower than the bubble point pressure, foamy oil is generated. The evolved gas doesn't coalesce together to form a gas phase, but rather a finely dispersed bubbles further destabilizes the sand particles and causes them to flow with oil. The free gas bubble entrained in the foam sustains reservoir pressure, resulting in anomalously higher oil productivity.

Having understood the mechanisms of CHOPS, it is imperative to find an efficient computational model that has the predictive capability to assist field operators to develop and monitor the optimal sand management and control strategies. A model should account for the effects of sand particle erosion, foamy oil behavior, and geomechanics. Ideally, predictions can assist oil producers in designing better pumping schemes for sand control, optimizing oil production, and ensuring wellbore stability.

The hydro-erosion model, first proposed by Vardoulakis et al.⁽⁶⁾, is based on rigid porous media (no skeleton deformation) in which mass balance is applied to a three-constituent system comprised of solid, fluid and fluidized solid using mixture theory. This model captured the erosion aspect of the unique process. Subsequently, Wan and Wang⁽⁷⁾⁽⁸⁾ extended this pure erosion model to include the effect of the deformation of porous media in a consistent manner. A single-phase flow formulation was fully coupled with geomechanics within a continuum mechanics framework. Furthermore, Wang et al.⁽⁹⁾⁽¹⁰⁾ extended previous work to a fully coupled reservoir-geomechanics model to account for the effects of multiphase flow and geomechanics for conventional light reservoirs. This approach results in solving a set of coupled non-linear time-dependent equations with fluidized solid concentration (saturation), fluid pressure, porosity, and deformation as main variables. The model has been proven to be a viable tool in terms of matching numerical calculations with lab test and field data⁽¹¹⁾. The volumetric oil and sand productions are calculated as a function of time, stresses, and hydrocarbon flow rate. Several cases in conventional oil reservoirs have been presented involving oilwell studies subject to different completion schemes (perforated casing and open-hole completion), water-cut effects, as well as three dimensional effects cases using the coupled reservoir-geomechanical model⁽¹²⁾⁽¹³⁾.

In this paper, we will extend this model to incorporate the foamy oil behavior for heavy oil reservoirs, and demonstrate its field application in terms of oil recovery and volumetric sand production.

Governing Equations For Coupled Multiphase Flow And Geomechanics With Erosion Mechanics

This model is based on mixture theory with erosion mechanics that is a common approach in continuum mechanics, in which multiphase hydrodynamics and geomechanics are coupled in a consistent manner via principal unknowns, such as saturation, pressure, porosity, and formation displacements. The porous media can be idealized as a Representative Elementary Volume (REV) that comprises of five phases, namely solid grains (*s*), fluidized solids (*fs*), fluid (*f*), water (*w*) and gas (*g*).

In reality, the individual distribution varies discontinuously over space. However, an averaging procedure in the spirit of mixture theory is used to homogenize each constituent over the REV volume V such that these individuals are substituted with continuous ones that fill the whole volume. Each phase discontinuity in the REV is represented in terms of its own volume fraction, i.e. saturation and porosity. For each phase, mass balance, equilibrium, and erosion mechanical equations can be derived. Full details of derivations can be found in Wang et al. ⁽¹²⁾. The set of governing equations are summarized as following.

Generalized reservoir mass balance equations

$$\nabla \cdot \left[\frac{\mathbf{v}_o}{B_o} + \frac{S_o \phi \dot{\mathbf{u}}_s}{B_o} \right] + \frac{\partial}{\partial t} \left[\frac{\phi S_o}{B_o} \right] = 0. \quad (1)$$

$$\nabla \cdot \left[\frac{\mathbf{v}_g}{B_g} + \frac{S_g \phi \dot{\mathbf{u}}_s}{B_g} + \frac{R_s \mathbf{v}_o}{B_o} + \frac{R_s S_o \phi \dot{\mathbf{u}}_s}{B_o} \right] + \frac{\partial}{\partial t} \left[\frac{\phi R_s S_o}{B_o} + \frac{\phi S_g}{B_g} \right] = 0. \quad (2)$$

$$\nabla \cdot \left[\frac{\mathbf{v}_w}{B_w} + \frac{S_w \phi \dot{\mathbf{u}}_s}{B_w} \right] + \frac{\partial}{\partial t} \left[\frac{\phi S_w}{B_w} \right] = 0. \quad (3)$$

Erosion mechanical equations

$$-\frac{\partial \phi}{\partial t} + \nabla \cdot [(1 - \phi) \dot{\mathbf{u}}_s] + \frac{\dot{m}}{\rho_s} = 0. \quad (4)$$

$$\frac{\partial [\phi (S_{fs} - 1)]}{\partial t} + \nabla \cdot [S_{fs} \mathbf{v}_m + (1 - \phi + S_{fs}) \dot{\mathbf{u}}_s] = 0. \quad (5)$$

Equilibrium equations

$$\nabla \cdot (\boldsymbol{\sigma}^{eff} - \omega P_m \mathbf{1}) + \mathbf{b} = \mathbf{0}. \quad (6)$$

The averaged mixture pressure can be defined as

$$P_m = S_o P_o + S_g P_g + S_w P_w \quad (7)$$

Foamy oil treatment

When the reservoir pressure drops below the thermodynamic equilibrium bubble point pressure, solution gas is liberated. In the conventional light oil case, the gas bubbles coalesce and grow rapidly to form a free mobile gas phase, while the gas bubble is entrained in the heavy oil situation due to high oil viscosity. In this paper, a simple approach is proposed to capture the uniqueness of foamy oil characteristics. We assume

the gas bubble never forms a free phase as the reservoir pressure drops below the bubble point pressure. We also assume the gas bubble moves with the same velocity as the oil phase. Essentially, foamy oil is treated like a single-phase flow with a modified formation volume factor B . The goal is to preserve the formation volume factor at different pressure levels. When the reservoir pressure is above bubble point pressure, the total formation volume factor

$$B_t = B_b [1 - c_f (P - P_b)] \quad (8)$$

While when the reservoir pressure is below bubble point pressure

$$B_t = B_o + (R_{sb} - R_s) B_g \quad (9)$$

Hence, the generalized reservoir mass balance equations (1-3) are reduced to two-phase equations, i.e. oil and water with a modified formation factor B_t .

Viscosity and permeability modification

Viscosity changes as the sand particles detach from the sand body and flow with fluid flow. Based on the law provided by Thomas relation, slurry viscosity is linked to fluid viscosity as a function of fluidized sand saturation, i.e.

$$\mu_s = \mu_f \{1 + 2.5 S_{fs} + 10 S_{fs}^2 + 2.7 \times 10^{-3} e^{(16.6 S_{fs})}\} \quad (10)$$

The permeability tensor can be related to porosity to account for the permeability enhancement via the variation of Carman-Kozeny equation or any lab-determined table based core analysis.

$$\mathbf{k} = k_0 \frac{\phi^3}{(1 - \phi)^2} \mathbf{1} \text{ or } \mathbf{k} = k_0 \exp \left[A \frac{\phi - \phi_0}{1 - \phi_0} \right] \mathbf{1} \quad (11)$$

Constitutive laws

Before above governing equations can be solved, constitutive laws describing sand particle erosion, fluid flow, and deformation of the sand matrix must be supplemented. It is commonly believed that the driving force causing the solid detachment from the sand matrix is due to hydrodynamics and geomechanics. Based on phenomenology, a possible functional form of mass generation can be extended from the inverse of filtration theory ^{(6) (14)}.

$$\begin{aligned} \frac{\dot{m}}{\rho_s} &= \lambda (1 - \phi) S_{fs} \left(1 - \frac{S_{fs}}{S_{fsc}} \right) \|\mathbf{v}_m\| & \text{if } \|\mathbf{v}_m\| \geq \|\mathbf{v}_m^{cr}\| \\ &= 0 & \text{if } \|\mathbf{v}_m\| < \|\mathbf{v}_m^{cr}\| \end{aligned} \quad (12)$$

As fluidized sand saturation increases, more suspended sand can be deposited due to their gravity. Therefore, erosion and deposition could balance each other when sand saturation reaches a critical value. The critical sand saturation S_{cr} prevents all the mass eroded away. The erosion coefficient λ provides a

length scale that can be linked to the accumulated plastic strains γ^p through the following relationship, i.e.

$$\lambda = \lambda(\gamma^p) = \lambda_0 + \frac{\gamma^p / \gamma_{\max}^p}{\alpha + \beta \gamma^p / \gamma_{\max}^p} \dots\dots\dots(13)$$

The average velocity of mixture is defined as

$$\mathbf{v}_m = w_o S_o \mathbf{v}_o + w_g S_g \mathbf{v}_g + w_w S_w \mathbf{v}_w \dots\dots\dots(14)$$

As for describing fluid flow, Darcy's law or non-Darcy's law is used to establish the relation between pressure gradient ∇p_j and discharge velocity \mathbf{v}_j for phases and the mixture. Turning to solid skeleton deformations, an elasto-plastic constitutive law incorporating dilatancy together with Drucker-Prager failure criterion is used to describe the behavior of the solid skeleton dominated by grain slippage, rearrangement, dilation and de-structuration under compression and shear ⁽¹⁴⁾.

Modular approach

Ideally, the coupled equations should be solved simultaneously due to the characteristics of their strong nonlinearity. However, it requires intensive computational power in terms of solving multiple variables at the same time. Moreover, it needs large code development and has difficulties of future maintenance. Over the past years, the authors have developed a practical and yet effective numerical strategy – Modular approach ^{(16) (17)}, which has prevailed due to its high efficiency, easy implementation, and above all accuracy if iterated to full convergence. Hence, an integrated iterative modular approach is adopted to incorporate this stress-flow-erosion model, of which current advanced standard reservoir and stress-strain codes are effectively taken advantage with minimum development efforts. More precisely, this model is reformulated into three integrated computational modules, i.e. erosion module, reservoir module, and geomechanics module. The communication of each module is fulfilled by the data passing among the interfaces of the modules, as shown in Figure 1.

The iterative method consists of the repeated solutions of the reservoir, erosion, and stress equations during the time step until certain convergence criteria are met. The iterative coupling could be time-consuming and computationally ineffective to achieve the same accuracy as the fully coupled solution ⁽¹⁶⁾. Hence, the implementation of this modular approach needs a robust interface among modules, where the computer memory handling and data passing take place. It is noted that the iteratively coupled method solves the problem as rigorously as a fully coupled (simultaneous) solution. The computational procedure is summarized as following.

(a) The reservoir module is solved to give pore pressure, temperature, and velocity of each phase profile based on boundary conditions and initial values.

(b) The geomechanics module is solved based on the pore pressure and temperature profile from (a) as load vectors. Sanding tendency (onset of sand production prediction) is monitored by checking whether the formation has failed in shear or tensile in this step. The erosion process weakens the solid matrix through degradation of its mechanical strength, i.e. Young's Modulus, friction angle, cohesion, etc. The geomechanics module calculates the volumetric changes, which can be related to porosity changes into the reservoir module.

The pore volume change is an important recovery mechanism accounting for a large part of the production. Another effect is the stress dependence of permeability ⁽¹⁷⁾, as the stress redistribution might alter the reservoir permeability as a result of isotropic expansion/compression and/or the creations of shear planes.

(c) Based on whether the critical velocity exceeds user-defined limits and whether the formation has failed, the erosion module is solved for two primary variables -- fluidized sand saturation and porosity. Plastic shear deformations, incurred in the solid matrix under fluid and stress gradients, increase the solid erosion potential in Equation (13). Porosity increases due to enhanced permeability, as described by the variation of Carman-Kozeny equation or a table developed from lab testing. In return, erosion activity intensifies with an increase of flow flux as the pressure distribution is modified in reservoir module. As the viscosity is altered due to the content change in the slurry fluid, the reservoir viscosity profile is also modified by fluidized sand saturation.

(d) With updated coupling terms from the geomechanics module and updated reservoir properties (permeability and viscosity) from the erosion module, the reservoir module is re-solved.

(e) Repeat (b) to (d) until certain convergence criteria are met. Then move to next time step.

It is worth mentioning that the Newton-Raphson scheme is used to speed up calculations in each module calculation to ensure each module converges quadratically with few limited steps. It is also noted that the calculation on sand initiation and production is automatically embedded in the computational procedure. Individual modules are triggered to solve for the primary variables once certain criteria are met. As the hydrocarbon production takes place, the erosion process begins as a result of the degradation of the sand matrix strength and the drag force imposed by fluid pressure gradient. The plastic yielding zones develop due to the material degradation (erosion) and stress re-distribution, while the wormholes or cavities form and propagate in terms of the increasing porosity values at intensive erosion range.

Numerical examples

In order to demonstrate the capacity of this model, typical vertical and horizontal wells from the Lindbergh and Frog lake fields in northeast Alberta, Canada are examined against field production data. The producing formations are composed of unconsolidated oil sand with a burial depth of 600 meters. It contains 12 – 14 API oil with in situ viscosities in the range of 3,000 to 10,000 cp. The initial pore pressure is around 4,000KPa, and bubble point pressure is about 3,500KPa. Core plug analysis showed virgin reservoir permeabilities in the range of 1,500-9,000md. Without significant sand, the average well produces a very slow oil rate less than 5m³/day ⁽¹⁸⁾.

Vertical well

In order to examine the generalized behaviors of heavy oil reservoirs, a quarter well with homogenized reservoir conditions is considered with a net pay of 6.1 meters in the vertical direction. Some basic reservoir data and modeling parameters are listed in Table 1. The drainage influence zone in the horizontal directions is 230 meters with a constant pressure support from outer boundaries. Dynamic time stepping is controlled by the reservoir module based on user-defined maximum and/or minimum changes of pressure, saturation, etc., in grid blocks. The simulation is carried out over 1000 days. Figure 2 shows the three-dimensional pressure distribution at

the end of 1000 days, while the plane view of pressure profile is shown in Figure 3. Due to the characteristics of compressive fluid, the oil tends to decrease at the beginning of production at a value of 1.7 m³/day. With the removal of sand particles, the permeabilities around wellbore increase, resulting in an enhanced oil rate up to 3.2 m³/day, as shown in Figure 4. It is noted that the quarter well rates should be multiplied by four to obtain the full well rates.

The lines with symbol in Figure 5&6 are the field data from each individual well. The average quarter well behavior shows cumulative gross fluid of about 2000 m³ with an associated sand production of 40 m³ within a production period of 1000 days. Despite the lack of real well operating constraints and detailed reservoir formation description, we can still match both the cumulative fluid and volumetric sand production history, as shown in Figure 5&6 (solid lines). Figure 5 also shows the foamy oil effects without sand (a line with triangle symbol) couldn't match the oil recovery by missing 50% oil production, while a good match can be made for both fluid and sand volume by accounting for the effects from sand production and foamy oil effects. Figure 6 shows a declining sand production with time to reach a constant value of 35 m³ as the sand particles adjacent to the wellbore are eroded out, while an oil recovery keep increasing to the value of 2150.9 m³ as shown in Figure 5. Figure 7 shows that porosity around wellbore gradually reaches the value of 0.8, while the fluidized sand saturation rises sharply to the value of 16% at the beginning, then declines to less than 2% over 1000 days. This typical phenomenon is commonly observed in field and lab test. Figure 8 is a porosity spatial plot along the distance from wellbore, showing that porosity increases over time around wellbore, and declines gradually away from wellbore. This indicates a progressively enlarged wellbore over time, which enhances oil recovery.

Horizontal well

A typical horizontal well is examined next to validate this model. This horizontal well lies 600 meters below surface with a total length of 250 meters. The horizontal permeability is 4.0 Darcy and 2.0 Darcy in the vertical direction. The well is operated at a minimum oil rate of 4 m³/day for the first 10 days, and then a minimum oil rate of 10 m³/day with a minimum bottom hole pressure at 500KPa through the simulation. The drainage influence zone is about 350m in diameter. The three-dimensional analysis over the total well length with various perforation intervals is possible, but computationally intensive. To simplify this issue, we assume that the horizontal well is uniformly perforated throughout the well, such that much-less-computational cost would be needed when the 3D computation is subject to 2D conditions.

Figures 9-11 show reservoir pressure distribution at selected times (10 days, 50 days, and 250 days). As the initial horizontal permeability distribution is two times larger than vertical ones, pressure declines elliptically around the wellbore. Accordingly, the porosity distribution follows the same trend as the most intensified erosion occurs in the regions of high-pressure gradient (Figures 12-14). Hence, in real reservoir conditions, the erosion tends to intensify in the higher permeability zone where fluid can easily flow, resulting in cavity growth and propagation in the higher fluid velocity zones.

Figure 15 shows the comparison of fluid rate between simulation and field data. The oil rate is boosted at the beginning of production by sand production. High sand cuts are observed at the beginning of production, as shown in Figure 16. As the reservoir pressure reduces below bubble point pressure, foamy oil plays a critical role in terms of maintaining reservoir pressure and destabilizing the sand particles. When the well is

turned to oil rate control, sanding declines substantially with a value of 0.5-1%. After 150 days' production, oil rate declines as the reservoir pressure starts to deplete. Over the 250 days period, the total amount of oil production is about 2376.7 m³, and the production of sand is around 67.2 m³. This is in a very agreement with field observation. It is interesting to find the cumulative fluid production is around 1767.7m³ by sand control (no sanding is allowed), which accounts only 74.3% of real oil recovery. This reason is that the removal of sand particles creates high permeable regions, causing viscous heavy oil flow easily, sustaining well at a high oil rate for a relatively long time. When no sand is allowed, the fluid rate is quite low even the bottom hole pressure is reduced to minimum value much faster than sanding case, as show in Figure 17.

Conclusion

This paper extended earlier work on sand production modeling to account for the foamy oil effect. This model is based on mixture theory with erosion mechanics, in which multiphase hydrodynamics and geomechanics are coupled in a consistent manner. Foamy oil is modeled as a dispersion of gas bubbles trapped in the oil, where these gas bubbles maintain a higher reservoir pressure. An integrated modular approach was also presented to effectively take advantage of the current advanced standard reservoir and stress-strain models. The mathematical model is implemented into three integrated computational modules, i.e. erosion module, reservoir module, and geomechanics module. The stress, flow and erosion equations are solved separately for each time increment. The coupling terms (porosity, permeability, plastic shear strain, etc.) are passed among them or iterated until convergence is achieved on a time step basis. The system is powerful in terms of its capabilities, yet practical in terms of the computer requirements.

Numerical results show that the enhanced oil recovery and volumetric sand production can be predicted by accounting for the effects of sand production and foamy oil behavior. It is found that there is an intimate interaction between foamy oil behavior and sand erosion activity. Porosity evolves in time and space as erosion progresses with initial drawdown. In turn the permeability of formations increases due to the porosity changes. This amplifies the erosion activity by virtue of increased flow rate. The self-adjusted mechanism enables the model to predict both the volumetric sand production and the cavity growth based on fluidized sand and porosity profile.

The model can be used for wellbore stability analysis and design in open-hole completions, perforation pattern design, as well as volumetric sand prediction with different pumping strategies to optimize the hydrocarbon production.

Acknowledgement

The authors wish to express their sincere gratitude for funding provided by Alberta Ingenuity Fund (AIF) and financial support from Halliburton Energy. The useful discussion with Mr. Bob Bachman is greatly appreciated.

NOMENCLATURE

ϕ	=	porosity
S_i	=	saturations ($i=o, g, w, fs$)
B_i	=	formation volume factors ($i=o, g, w$)
ρ_i	=	densities at stock tank condition
\mathbf{v}_i	=	velocity of each phase ($i=o, g, w, fs$)

R_s	=	solution gas oil ratio
$\dot{\mathbf{u}}_s$	=	volume-weighted velocity of deforming solid skeleton
\dot{m} / ρ_s	=	source or sink term to account for the local rate of solid loss or gain per unit volume
$\boldsymbol{\sigma}^{eff}$	=	effective stress
\mathbf{b}	=	body forces per unit volume
ω	=	Biot coefficient
$\mathbf{1}$	=	Kronecker delta tensor
\mathbf{v}_m^{cr}	=	critical average velocity of mixture below which no sand production occurs
α, β	=	constants to be determined
λ_0	=	erosion coefficient
γ_{max}^p	=	maximum plastic shear strain
w_j	=	weighting factors which can be determined from rock wetness($j=o, g, w$)
μ	=	viscosity

REFERENCES

1. TREMBLAY, B., SEDGWICK, G., AND VU, D., *CT imaging of wormhole growth under solution – gas drive*, *SPE Reservoir Engineering Journal*, 2, pp. 37-45, 1999
2. SAWATZKY, R.P. AND LILICO, D.A., Tracking cold production footprints, *CIPC, Calgary, Alberta*, 2002.
3. DUSSEAULT, M.B., AND EL-SAYED, S., Heavy oil well production enhancement by encouraging sand influx, *paper SPE 59276, the SPE/DOE Improved Oil Recovery Symposium, Tulsa, OK, 305 April, 2000*.
4. JOSEPH, D., KAMP, A., AND BAI, R., Modelling foamy oil flow in porous media, *Int. J. Multiphase Flow* 28, pp. 1659-1686, 2002.
5. Maini, B.B., Sarma, H.K., and George, A.E., *Significance of Foamy-Oil Behaviour in Primary Production of Heavy Oil, JCPT (November 1993) 50*.
6. VARDOULAKIS, I., STAVROPOULOU, M. AND PAPANASTASIOU, P., Hydromechanical aspects of the sand production problem. *Transport in Porous Media*. 22, 225-244, 1996.
7. WAN, R.G. AND WANG, J., Modelling sand production within a continuum mechanics framework. *Journal of Canadian Petroleum Technology*. 41:4, 46–52, 2002.
8. WAN, R. G. AND WANG, J., Modelling sand production and erosion growth under combined axial and radial flow. *SPE International Thermal Operations and Heavy Oil Symposium and International Horizontal Well Technology Conference SPE 80139. Calgary, Canada, 4–7 November 2002*.
9. WANG, J. AND WAN, R. G., Computation of sand fluidization phenomena using stabilized finite elements, *Finite Elements in Analysis and Design* 40:1681-1699, 2004.
10. WANG, J., WAN, R.G., A. SETTARI, WALTERS, D.A. AND LIU, Y.L., Sand production and instability analysis in a wellbore using a fully coupled reservoir-geomechanics model, *Gulf Rocks 2004, the 6th North America Rock Mechanics Symposium (NARMS): Rock Mechanics Across Borders and Disciplines, held in Houston, Texas, June 5 – 9, 2004*.
11. WAN, R.G. AND WANG, J., Numerical modeling of sand production in an oil well of the Messla field. *Research Report Submitted to Golder Associates, 36p, 2004*.
12. WANG, J., WAN, R.G., SETTARI, A., AND WALTERS, D.A., Prediction of volumetric sand production and wellbore stability analysis of a well at different completion schemes. *Alaska Rocks 2005, the 40th U.S. Symposium on Rock Mechanics (USRMS): Rock Mechanics for Energy, Mineral and Infrastructure Development in the Northern Regions, held in Anchorage, Alaska, June 25-29, 2005*.
13. WANG, J., WALTERS, D.A., SETTARI, A., AND WAN, R.G., An integrated modular approach to modeling sand production and cavity growth with emphasis on the multiphase flow and 3D effects. *Golden Rocks 2006, The 41st U.S. Symposium on Rock Mechanics (USRMS): "50 Years of Rock Mechanics - Landmarks and Future Challenges", held in Golden, Colorado, June 17-21, 2006*.
14. STAVROPOULOU, M., PAPANASTASIOU, P. AND VARDOULAKIS, I., Coupled wellbore erosion and stability analysis. *Int. J. Numer. Anal. Methods Geomech.* 22, 749-769, 1998.
15. WANG, J., Mathematical and numerical modeling of sand production as a coupled geomechanics-hydrodynamics problem. *Calgary. (PH. D. dissertation), 2003*.
16. AZIZ, K, AND SETTARI, A., Petroleum reservoir simulation. *London. Elsevier Applied Sci., 1979*.
17. SETTARI, A. AND WALTERS, D.A., Advances in coupled geomechanical and reservoir modeling with applications to reservoir compaction. *SPE Journal*. 9: 334–342,2001.
18. METWALLY, M., and SOLANKI, S.C., Heavy Oil Reservoir Mechanisms, Lindbergh and Frog Lake Fields, Alberta. Part I: Field Observations and Reservoir Simulation; *Paper 95-63, 46th Annual Technical Meeting of The Petroleum Society, Banff, AB, May 14 – 17, 1995*.

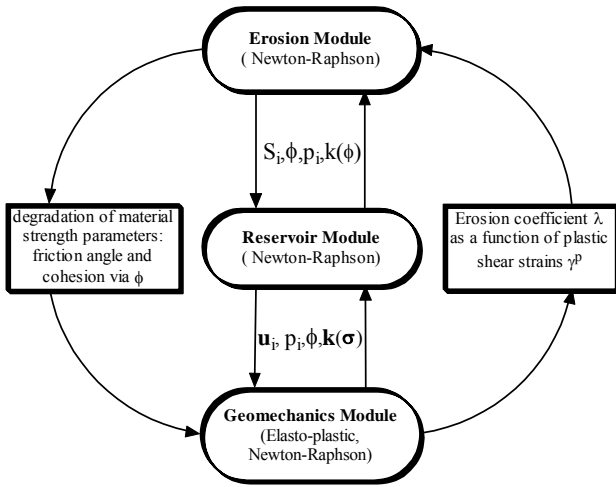


Fig. 1. Schematic of the coupled system architecture.

Table 1 Basic reservoir data and model parameters

$\lambda = 1.1 \text{ m}^{-1}$	$\rho_s = 2.67 \text{ g/cm}^3$	$\rho_o = 0.98 \text{ g/cm}^3$
$\rho_w = 0.97 \text{ g/cm}^3$	$c_o = 6.4\text{E-}07/\text{KPa}$	$c_w = 4.6\text{E-}7/\text{KPa}$
$K_0 = 8.5 \text{ Darcy}$	$\mu = 3,000 \text{ cp}$	$\phi = 0.32$

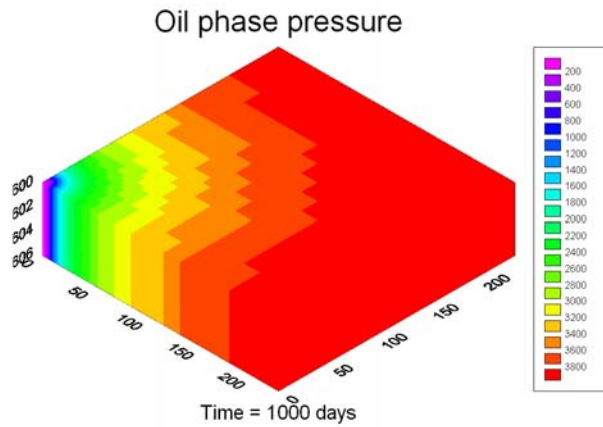


Fig. 2. 3D pressure distribution at time 1000days.

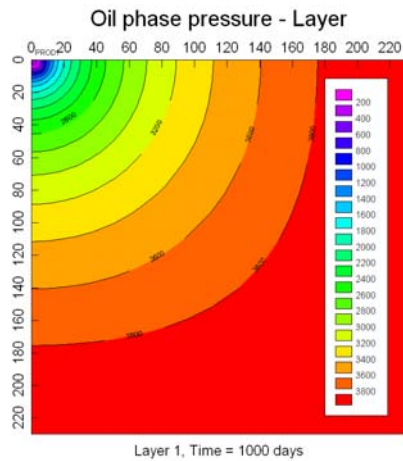


Fig. 3. Plane view of pressure profile at time 1000 days.

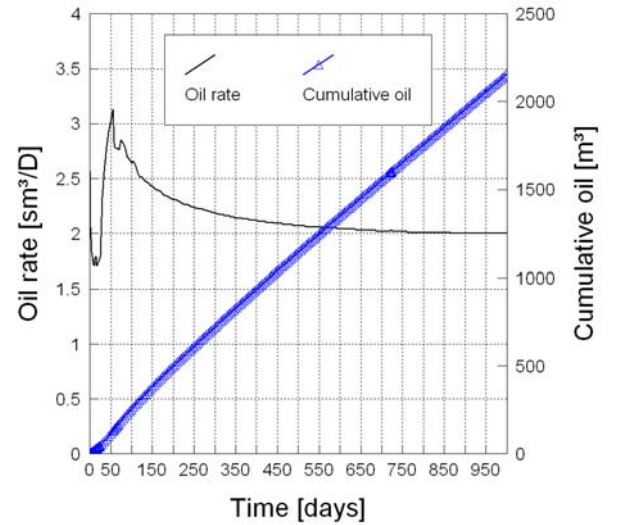


Fig. 4. Oil rate history and cumulative oil production.

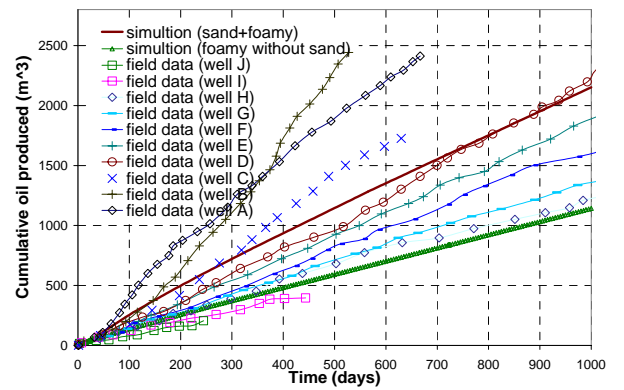


Fig. 5. Cumulative oil production history match.

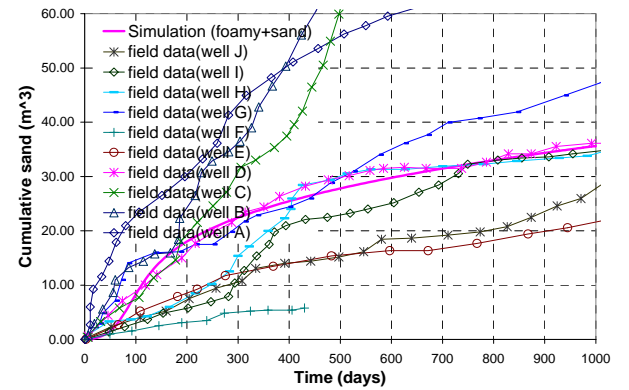


Fig. 6. Cumulative sand volume history match.

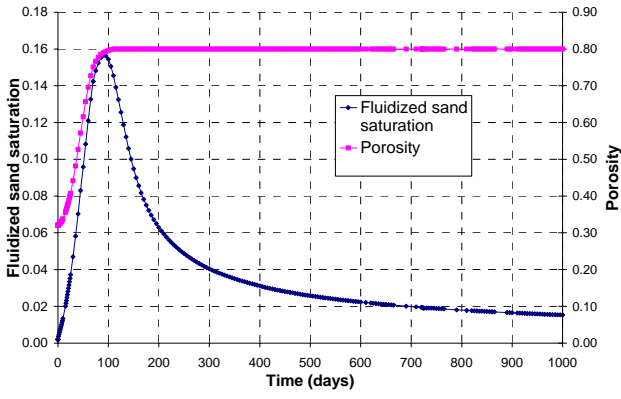


Fig. 7. Fluidized sand saturation and porosity profiles at wellbore.

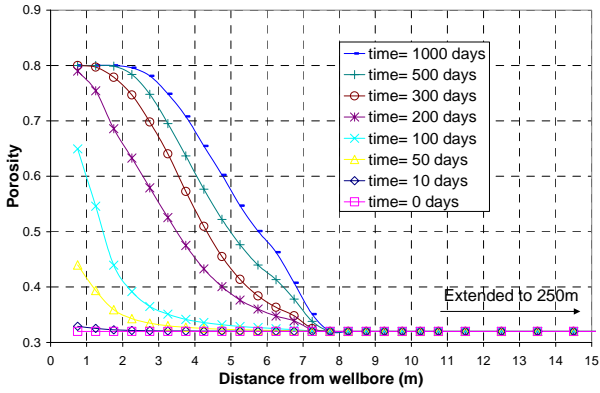


Fig. 8. Porosity profiles at selected times.

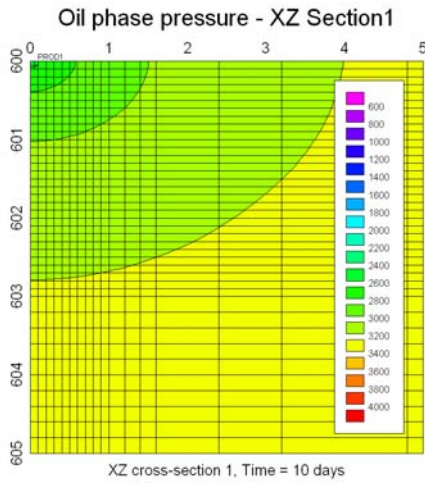


Fig. 9. Pressure distribution at time 10 days.

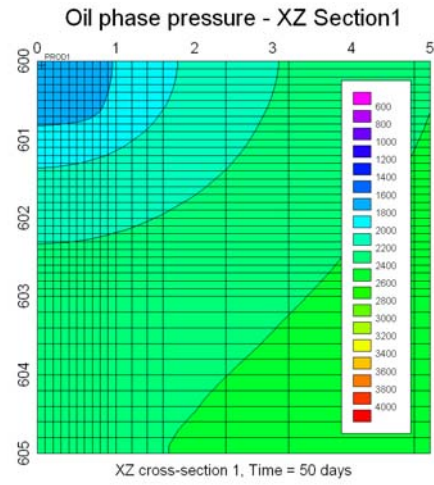


Fig. 10. Pressure distribution at time 50 days.

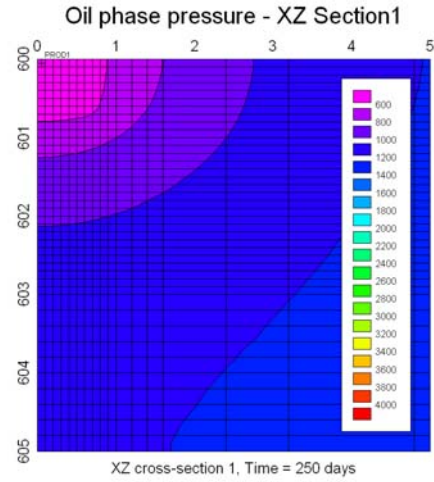


Fig. 11. Pressure distribution at time 250 days.

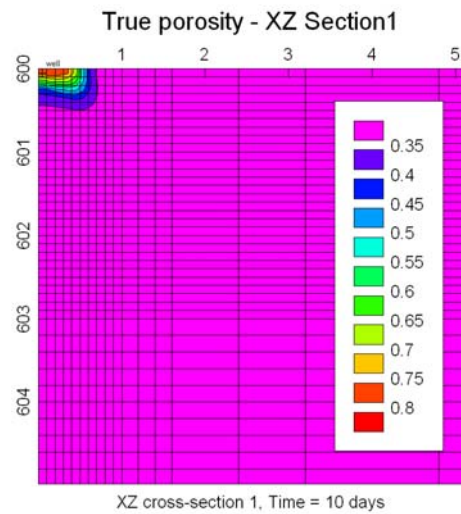


Fig. 12. Spatial porosity distribution at time 10 days.

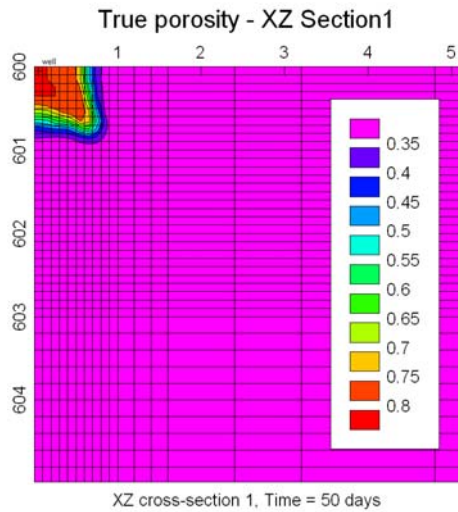


Fig. 13. Spatial porosity distribution at time 50 days.

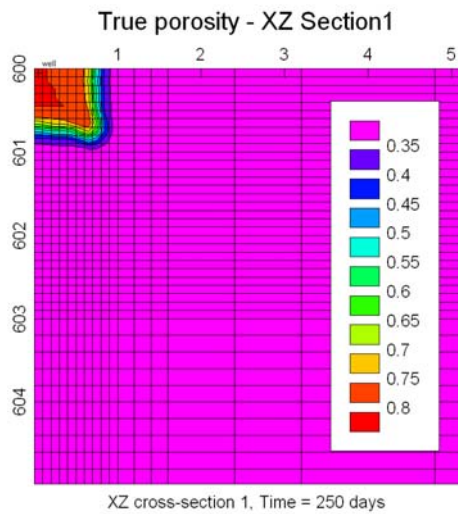


Fig. 14. Spatial porosity distribution at time 250 days.

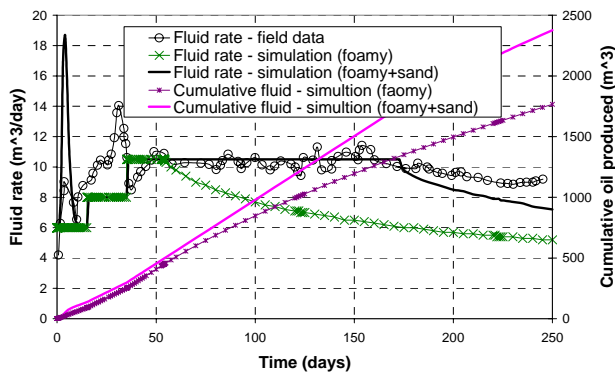


Fig. 15. Comparison of fluid rate and cumulative oil production.

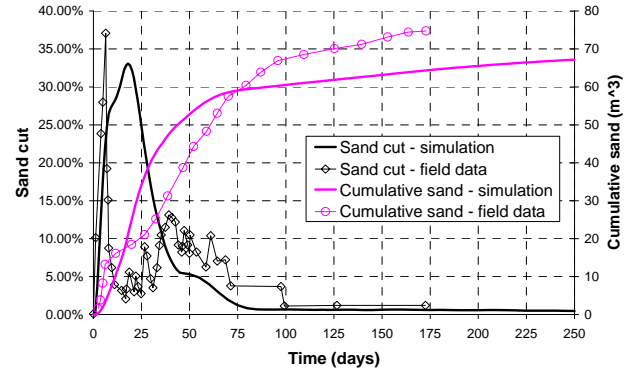


Fig. 16. Comparison of sand cut and cumulative sand production.

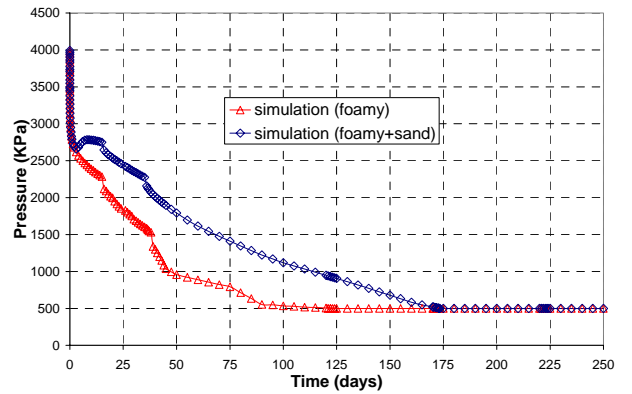


Fig. 17. Bottom hole pressure comparison.